

## Flood and Sediment Disasters Triggered by 1999 Rainfall in Venezuela; A River Restoration Plan for an Alluvial Fan

Tamotsu TAKAHASHI\*, Hajime NAKAGAWA\*, Yoshifumi SATOFUKA\* and Kenji KAWAIKE\*\*

\*Disaster Prevention Research Institute, Kyoto University

\*\*Graduate Student, Graduate School of Engineering, Kyoto University

(Received for 31 Aug., 2001)

### ABSTRACT

Severe rainfall during December 1999 triggered numerous landslides, debris flows, and flash floods on the Caribbean coast of Venezuela, resulting in a great number of deaths estimated as between 25,000 and 50,000. The natural as well as social conditions that led to this severe disaster were analyzed. A combination of bad conditions was seen as the cause. A numerical simulation method for reproducing phenomena that occur on an alluvial fan is introduced. It was verified by a comparison of the calculated results with actual situations. This simulation method was used to assess the efficacy of possible countermeasure plans. A combination of sabo dams and channel works was found effective on the fan of the Camuri Grande River.

### 1. INTRODUCTION

Continuous severe rainfall from 8 to 19 December 1999 caused disasters in the eight states of northern Venezuela. The state of Vargas, located on the northern slopes of the Cordillera de la Costa mountain range, was the most severely damaged by landslides, debris flows, and flash floods induced by concentrated rainfall from 15 to 16 December.

The official statistics of damage compiled by the Civil Defense Agency of the state of Vargas at the time of our reconnaissance in March 2000 were as follows (Maki, 2001): Affected houses, 40,160; completely collapsed houses, 20,000; affected persons, 214,000; injured persons, 2,700; dead persons, 248; missing persons, 2,850; refugees, 43,569. The media and local governments, however, estimate the lives lost as 25,000 to 50,000, and the International Red Cross makes it as high as 30,000. The reason for the wide range in the death toll is due to the non-availability of census data and difficulties in recovering bodies from under thick rocky debris or deep in the sea. This disaster is said to be the worst to have occurred in Latin America in the 20th century.

A reconnaissance team consisting of five specialists from various fields was dispatched to Venezuela in March 2000 by the Japanese Ministry of Education, Science, Sports and Culture. Its official report has been published (Takahashi et al., 2001). This paper is not a comprehensive summary of the official report, rather it focuses on the natural and social conditions that resulted in the disasters, makes a comparison with Japanese disasters that suggest effective countermeasures, gives a theoretical reproduction of flooding on the fan of the Camuri Grande River, and theoretical examinations of several river restoration plans on that fan. Of the four authors of this paper, the first two carried out the field investigations and the latter two collaborated with them in making the numerical simulations.

### 2. NATURAL CONDITIONS THAT PRODUCED HAZARDS

The state of Vargas is long and narrow and faces the Caribbean Sea on the north. It is separated from Caracas to the south by the high Cordillera de la Costa mountain range. The central part, the most severely devastated area, is shown in Fig. 1. The distance from the coast to the ridge is about ten kilometers, and the altitude of the ridge is between 2,000 and 2,700m, therefore the northern slopes of the mountain range have an average steepness of 10 to 15 degrees. The major rivers shown in the figure have formed alluvial fans adjacent to the coast, but the rest of this coastal zone area consists of steep mountain fronts rising directly from the shoreline. These alluvial fans provide the only relatively flat areas, at first glance suitable to live on, but they are by no means safe. Towns, however, have been constructed on these fans, and a road hugging the steep mountain fronts along the coast connects these towns.

The geological setting of this area has the general trend of a belt-like formation parallel to the Caribbean coastline (Chigira, 2001). The zone, about 1.5km wide on the coast, is "mélange" consisting mainly of calcareous phyllite. The phyllite has been heavily weathered to clayey materials and forms steep slopes of 25 to 40 degrees that face the sea. Because this zone contains much clay, water permeability is low. Vegetation in this zone is, perhaps due to human activity, poor, mostly sparse shrubs and cactuses. The roots of these types of vegetation are only 20 to 30cm deep. To the south of this zone, schist and granitic gneiss zones form the main parts of the mountains.

In December 1999, because of a cold front that lingered for about twenty days along the Caribbean coast, rainfall at the Maiquetia airport totalled 1,207mm. For the three days from the 14th to 16th 914mm of rainfall was recorded. Rainfall records from 1951 to 1997 at Macuto about 10km east of Maiquetia, show

an annual mean rainfall of 589mm.

Although the ground level rainfall record is available only for Maiquetia airport, the homepage of the USGS-CINDI (Center for Integration of Natural Disaster Information) gives a two-dimensional distribution of rainfall from 15 to 17 December based on automatic estimation of GOES-8 satellite data (USGS-CINDI team, 1999). According to the record at Maiquetia, the rainfall on 17 December amounted to only 2.9mm. In practice, therefore, the distribution map of CINDI shows the amount from 15th to 16th. The rainfall estimated by CINDI at Maiquetia is 300 to 480mm. The rain gauge record at Maiquetia for this period gives 774mm. To cancel out the difference between these data, the rainfall estimated by CINDI was modified by multiplying by a factor of 1.9,

and the distribution map was enlarged, giving the isohyetal map in Fig. 2. Although the accuracy of this isohyetal map is poor due to the extreme enlargement and marked modification of the estimated values, the general rainfall distribution tendency can be understood.

Figure 2 shows that the most severe rainfall was in the Macuto area, decreasing to the east. It also shows that the strongest rainfall was along the coast, weaker in the higher mountain areas. This situation is indirectly supported by the fact that, in the Caracas area on the opposite of the mountain ridge, no severe flooding occurred.

The characteristic geological and rainfall distributions described above therefore must be the main factors that determined the distributions of the numbers and positions of landslides and

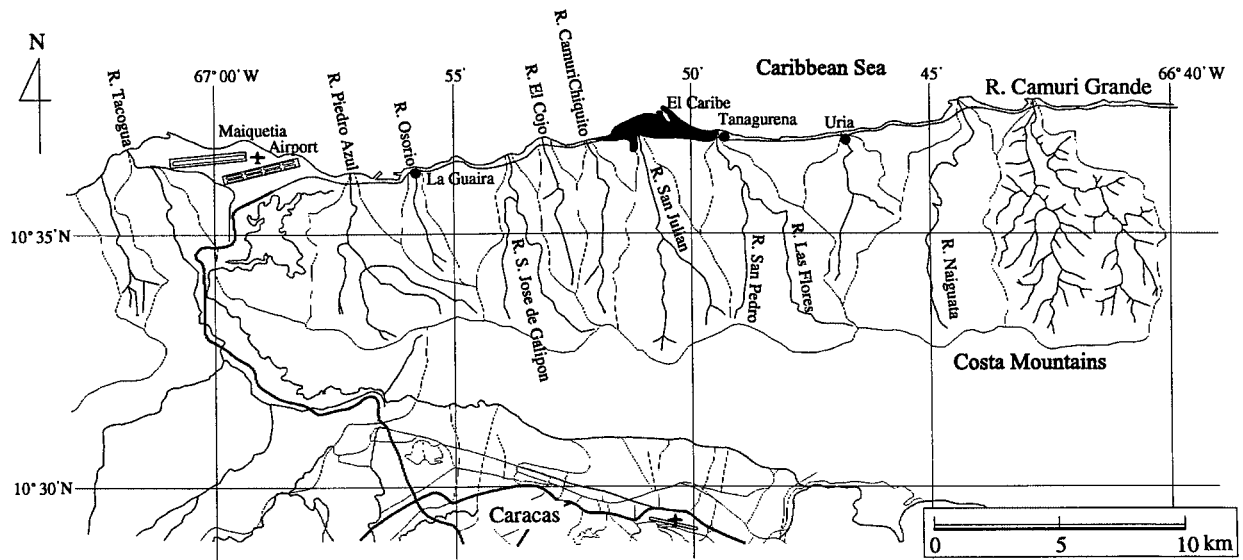


Fig. 1 Central part of the state of Vargas and metropolitan Caracas.

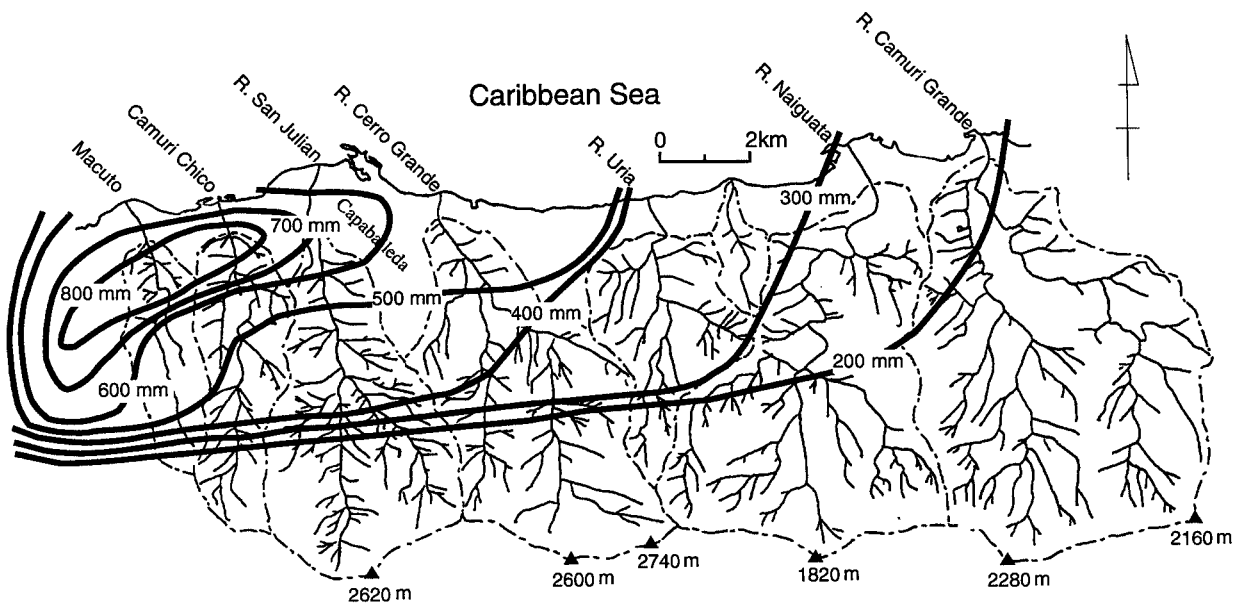


Fig. 2 Major river systems and isohyetal lines of the rainfall

debris flows. As seen in Photo 1, landslide density is very high in the mainly weathered phyllite hilly area along the coast. Although landslide density is very high, the scale of the respective landslides is small; about 20m wide, less than 100m long and shallow. The main road constructed along the coast was littered with the deposits of landslides, and its function destroyed. The very dense landslide area, however, is almost completely to the west of the Naguayata River. This situation correlates well with the decrease in the rainfall to the east.

Landslides that occurred on schist and gneiss slopes were a kind of rockslides, and many of their scars are connected with riverbeds. Little debris remains on these scars or the riverbeds. The landslide density on these slopes is much lower than in the former area. Presumably this is because these areas are covered with good vegetation and the rainfall was less than in the coastal area.

Dark colored sands, derived from landslides in the phyllite zone, cover the narrow beaches at the foot of the steep mountain front, whereas white sands, gravel, and boulders derived from granitic gneiss areas cover the alluvial fans of the major rivers (Fig. 2). They were transported to the fan area by debris flows or flash floods. The shorelines of the alluvial fans have advanced offshore about 200m.



Photo 1. Densely distributed landslides on steep phyllite slopes near the coastline.



Photo 2. A shantytown on a very steep, weak slope.

### 3. SOCIAL CONDITIONS THAT RESULTED IN CATASTROPHIES

The Venezuelan population is estimated to be 23.5 million, and the land area 912 thousand square kilometers. About 75% of the land consists of the tropical rain forest of the Orinoco River basin, and most of the population lives in the northern highlands and valleys. The capital city, Caracas, is on a 900m-high basin and has about 10% of the country's population. Congested slums occupy the mountain slopes that surround the Caracas basin.

The central part of the state of Vargas is separated from the metropolitan Caracas by a very high mountain range (Fig.1), but is easily accessible from Caracas via a pass. Maiquetia, the principal international airport of Venezuela, and La Guaira, a major trading seaport, are located in this state. Due to these advantageous geographical conditions and the state's beautiful coastal and mountain settings, the alluvial fans of the major rivers located between the foot of mountain range and the coast have been highly developed as resort towns. Development of the area has caused an inflow of people for employment. These newcomers could not find flat land suitable for building, so many shantytowns have been constructed on very steep slopes highly vulnerable to landslides near the developed alluvial fans (Photo 2) or on canyon bottoms clearly vulnerable to floods (Photo 3). Luxurious high-rise hotels and condominiums, yacht harbors, and slums constitute the strange, characteristic scenery of this area. These towns were the main sites of the disasters.

### 4. PRINCIPAL TYPES OF DAMAGE

#### 4.1 Destruction due to direct landslide strikes

As stated, low-income people are obliged to live on highly hazardous land, typically on the very steeply sloping areas of the mountain fronts that rise directly from the Caribbean Sea and side slopes of developed alluvial fans. Because the landslide density in these areas is very high, as is the density of the houses constructed, these houses had high probability to be struck by falling earth blocks or to undergo the sliding of the ground on which they were built. Some houses were destroyed by the collapse of houses above them. Poor drainage systems in these shantytowns also could trigger landslides.



Photo 3. A shantytown on a canyon bottom.

Because the speed of weathering in this phyllite area is rapid and unstable slopes remain around the scars of landslides, these areas are highly vulnerable to similar future disasters.

#### 4.2 Obliteration due to debris flow flooding on canyon bottoms

Narrow canyon bottoms between steep walls were filled with numerous low-income houses which were obliterated by debris flows exceeding the entire canyon's width. Some houses were hit directly and destroyed by landslides that occurred on the canyon walls. This type of damage occurred along the Cerro Grande (Photo 4) and Uria rivers (Photo 5).

In the former, about a 800m long, 200m wide reach immediately upstream of the fan-top, forms a canyon plain, which was crowded with numerous houses, except for a narrow channel that drained away the normal river water. Almost all these houses were swept away by a debris flow.

In the latter, a long stretch of the coastal cliffs had been abruptly hollowed out, forming a canyon 700m long and 220m wide at the mouth of the Uria River. This plain was completely covered by a shantytown, Carmen de Uria (Photo 5). Its two central blocks were obliterated by debris flows (Photo 5). The houses remaining are by no means safe (Photo 6). More than five thousand people are said to have been killed in this town.



Photo 4. Situation before and after the disaster at Cerro Grande



Photo 5. Situation before and after the disaster at Carmen de Uria

### 4.3 Damage due to flooding by debris flows/flash floods

Typical examples can be seen on the alluvial fans of the San Julian (Caraballeda) and Camuri Grande (Camuri Grande) rivers.

The former fan was swept by several debris flows which left a cover 1.2km<sup>2</sup> wide and a few meters-thick deposit that included boulders 2 to 3 meters in diameter. This fan, the largest in the central part of Vargas, has been highly developed as a resort town, and has many high-rise hotels and condominiums with small individual houses between them (Photo 7). Many lower situated houses were flushed away or buried to the roof, and some high-rise concrete buildings partly collapsed because of being hit by big boulders (Photo 8).

Photo 9 shows the Camuri Grande alluvial fan. A tributary, the Miguelena River, with the same comparative scale as the main river, joins it near the fan-top, but sediment runoff from that tributary was little. The sediment that covered the fan therefore almost all was from the main Camuri Grande River. The main river channel changes direction perpendicularly eastward immediately upstream of the fan-top, and, after joining the Miguelena River, it again changes direction perpendicularly northward. Thus, the river channel has a "crank" shape that creates an obstacle to flood flow. On the left side of this crank channel (looking downstream) is the campus of Simon Bolivar University.

A debris flow that carried many boulders more than 1m in diameter stopped in the upstream region of the confluence with the Miguelena River, and the subsequent flash flood spilled over the deposit and separated in two. One overflowed the main channel before entering the crank channel and continued to flow straight into the university campus, destroying buildings or burying them to the roof. This flow bore much large woody debris.

Some of the flow that spilled over the debris flow deposit followed the crank channel and joined the flood flow from the Miguelena River. Part of that flow overflowed the right bank of the channel in the neighborhood of the second change in direction. It buried the first floors of a group of reinforced concrete apartments near the channel bend then continued its run down along the mountain foot to the sea destroying and burying numerous small houses.

The rest overflowed and continued along the crank channel destroying houses along the main connecting road with other towns then flowed out to the sea, extending the coastal line about 250m off shore.

The diameters of the sediment grains deposited on the fans of the San Julian and the Camuri Grande rivers differed, and the damage aspects also differed. Very large boulders predominated, and the destructive power of the flow was much greater on the fan of



Photo 6. Destroyed houses at Carmen de Uria



Photo 8. Building collapsed due to the direct strikes by boulders.



Photo 7. Alluvial fan of the San Julian River



Photo 9. Alluvial fan of the Camuri Grande River

the San Julian than on the fan of Camuri Grande River. Many houses on the San Julian fan were obliterated, and even concrete buildings collapsed, whereas on the Camuri Grande fan the majority of the houses were buried by sand. To clarify the reasons for these differences, longitudinal profiles of the main channels of these rivers are shown in Fig. 3, in which altitudes and distances from the river source are standardized to the height of the source of the San Julian River, 2170m. Profiles of the Uria, Cerro Grande, and Naiguata rivers are compared in the same figure. Damage on the Naiguata fan was not slight, but it was the least in these five river basins. Figure 3 shows that every river channel is steeper than the slope of the debris flow generation limit (15 degrees) in the upstream reaches. All these rivers actually produced debris flows. Arrows show the positions of the upstream limits of residential areas in these river basins. In order, residential areas in the Uria, Cerro Grande and San Julian basins are closer to the debris flow generation reach and are on land steeper than 3 degrees through which large scale debris flow can pass. In contrast, the residential areas on the Camuri Grande and Naiguata fans are far from the debris flow generating reach, flatter than 2 degrees which debris flows do not reach (Takahashi, 1991).

## 5. COMPARISONS WITH JAPANESE SITUATIONS

Is this Venezuelan disaster unparalleled in history in terms of natural phenomena? To answer this question and to evaluate methods for restoration, the phenomena are compared with Japanese ones.

Figure 4 shows the relationship between specific sediment yields and basin area for the seven rivers in Vargas and the same relationship in conspicuous Japanese cases (Mizuyama, 1985). Because the exact sediment yield volumes from the Vargas rivers are not known, a rough approximation was made by multiplying the area of sediment flooding obtained from aerial photographs by 2m. This figure shows that although the sediment yields from the major rivers in Vargas are of the largest scale, they are not markedly larger than those in the Japanese examples. That is, this scale sediment runoff has to be taken into account when planning countermeasures in such debris flow-prone river basins.

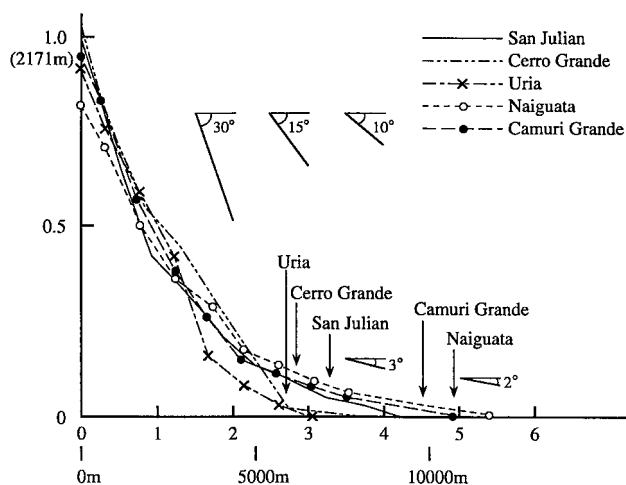


Fig. 3 Longitudinal profiles of the major rivers and positions of upstream boundaries of residential areas

Resemblances in topography and the hazard areas recall the disaster of 1938 in Kobe district, Japan, called the great Hanshin flood disaster. Figure 5 shows the river networks originating in the Rokko mountain range, the cumulative rainfall distribution from July 3 to 5 1938, and the main sediment deposition areas. Comparison of this figure with Fig. 2, shows the resemblance between the conspicuous disaster range and distance from the coast to the mountain ridge. The highest peak of the Rokko Mountains is only 931m, whereas that in Vargas is 2,740m. In Vargas, the mountains are very close to the coast, whereas at Rokko the torrent outlets are 2 to 3km upstream from the river mouths. The longitudinal inclinations of the torrents inside Rokko Mountain are similar to those in Vargas, therefore sediment transportation in Rokko should be similar to that in Vargas. The total sediment volume in Rokko is estimated as  $5 \sim 7.7 \times 10^6 \text{ m}^3$  and that from the major Vargas rivers of the order of  $6 \sim 7 \times 10^6 \text{ m}^3$ . The sediment volumes were similar, but the damage in Rokko was much less: 616 died, 1,410 houses were obliterated, 854 houses were buried, and 2,213 houses were partly destroyed. These differences presumably are due to the fact that at that time developed areas in the Rokko area were limited to flat zones distant from the outlets of the gorges.

After the 1938 disaster, as structural countermeasures, sabo dams were intensively constructed. Totally, 174 sabo dams had been finished when a matching rainfall event struck the same district in 1967. In 1967 the number of landslides was similar to that in 1938, but due to the functioning of the sabo dams only  $0.5 \times 10^6 \text{ m}^3$  of sediment flowed down to the alluvial fans, and other  $0.17 \times 10^6 \text{ m}^3$  overflowed river channels downstream. In the 1967 disaster, 98 people died and 363 houses were completely destroyed. Whereas in 1938, the majority of injuries and deaths were downstream of the outlets of the gorges, in 1967, people died inside the mountain area because by then residential areas extended well into the mountain. One must take into account that the upgrading of preparedness for disasters by the construction of structural countermeasures, sometimes, expecting too much of these structure's functions, increases the number of people living in dangerous zones.

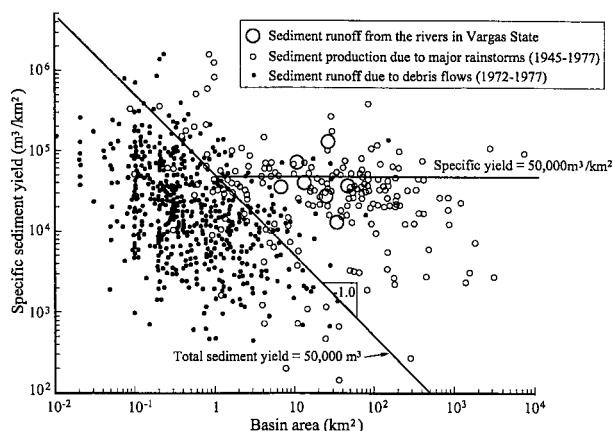


Fig. 4 Relationship between specific sediment yields and basin area

## 6. COUNTERMEASURES AGAINST FUTURE DISASTERS

Our reconnaissance showed that little sediment remains on the upstream riverbeds of the major Vargas rivers. Until considerable sediment is accumulated no episodic event comparable to that of 1999 will occur. The sediment volume in the 1999 event is, however, not especially large when compared with other episodes. The matching volume of sediment runoff therefore should be taken into account when planning countermeasures.

A priority policy should be the removal of slums built on the very steep slopes close to the coastal area. The president of Venezuela announced as early as Dec. 20, 1999 that permanent resettlement sites would be prepared in some remote states with agricultural land and housing for the disaster victims (Maki, 2001). Because many of those people had been living in these slums to escape the hardships of life in remote states, the success of this policy is questionable.

The canyon plains of the Uria and Cerro Grande rivers will not be suitable residential areas unless sabo dams of sufficient capacity are constructed.

The alluvial fan of the San Julian River has a slope that allows large scale debris flow passage. Therefore, if a channel with sufficient conveyance capacity is constructed, most of the alluvial fan area will mostly become safe. Debris flow material, however, will necessarily be deposited at the river mouth and deposition will tend to go up the channel. A sand-pocket or sabo dam to store excess debris will be necessary.

Debris flows in the Naiguata and Camuri Grande rivers will stop upstream of the fantop, and immature debris flows or flash floods will run down to the fan area. Such flows will deposit material within the flat reach of channel works before flowing into the sea. Sabo dams of sufficient capacity therefore are needed upstream of the fan-top.

The efficiency of such structural countermeasures must be evaluated quantitatively by computer simulation as described

below.

## 7. PROPOSED COUNTERMEASURE PLAN FOR THE CAMURI GRANDE BASIN

### 7.1 Estimation of debris flow hydrograph in the river basin

For the design of countermeasures, a debris flow event equivalent to that of 1999 is needed. Because no quantitative data for the debris flow that caused that disaster are available, the first thing is to determine the design debris flow quantitatively; i.e., reproduction of the phenomena by computer. The simulation model used combines flood runoff analysis by the kinematic wave method and sediment runoff analysis based on various fundamental equations (Takahashi et al., 2001a).

#### 7.1.1 Fundamental equations for routing highly sediment-laden flow

- (1) Equations used in flood runoff analysis by the kinematic wave method

Flood runoff analysis of a mountain slope can be made by the kinematic wave runoff model:

$$q_s = \alpha_k h^{5/3} \quad (1)$$

$$\alpha_k = \sin^{1/2} \theta_s / n_e \quad (2)$$

$$\frac{\partial h}{\partial t} + \frac{\partial q_s}{\partial x} = r_e \quad (3)$$

where  $q_s$  = water discharge per unit width,  $h$  = water depth,  $\theta_s$  = slope gradient,  $n_e$  = equivalent roughness coefficient,  $r_e$  = effective rainfall intensity,  $t$  = time, and  $x$  = distance from the slope's top.

Neglecting the increase and decrease in discharge due to erosion and the deposition of sediment, flood runoff analysis in the river channel is made by the following equations:

$$q = \frac{1}{n_m} h^{5/3} \tan^{1/2} \theta_w \quad (4)$$

$$\frac{\partial h}{\partial t} + \frac{1}{B} \frac{\partial q B}{\partial x} = \frac{q_s}{B} \quad (5)$$

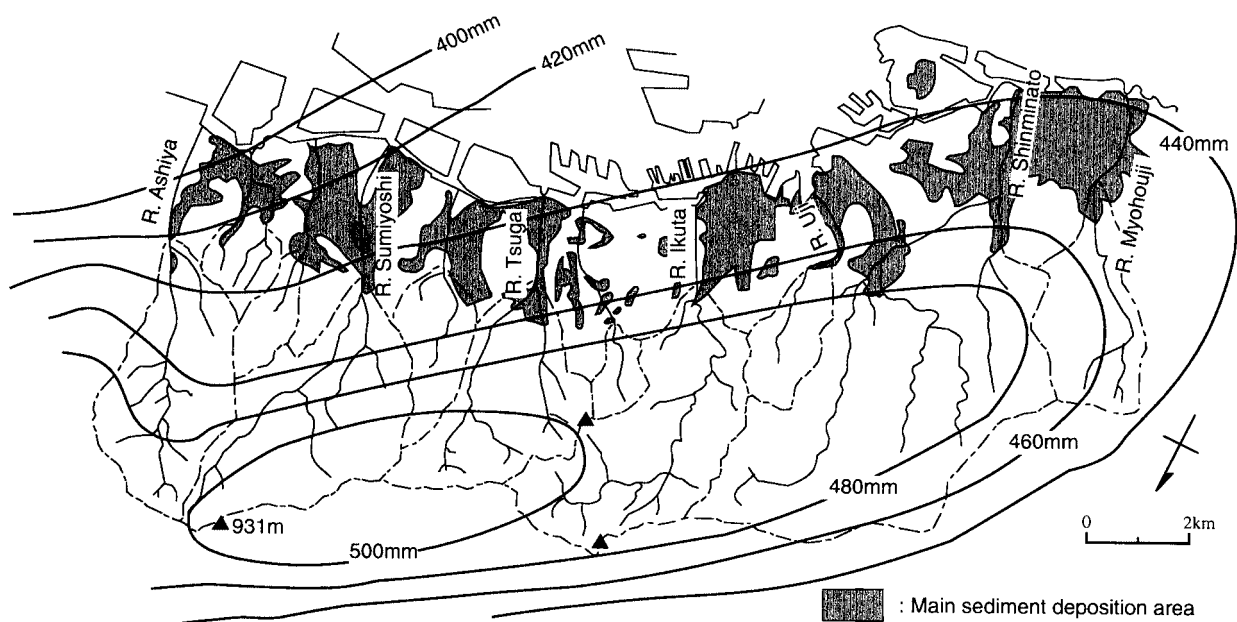


Fig. 5 Sediment disaster of 1938 Kobe district, Japan

where  $q$  = water discharge per unit width of river channel,  $n_m$  = Manning's riverbed roughness coefficient,  $B$  = channel width, and  $\theta_w$  water surface gradient.

(2) Equations giving the competence of flow to carry sediment

Erosion and deposition are neglected in the flood runoff analysis, but, actually, the riverbed material together with confined water within the bed will be entrained into flow, provided the load is still below the competence of flow and erosion takes place. In contrast, if the competence of flow is insufficient to transport the load, sediment will be deposited. Therefore, erosion and deposition will change the flow discharge and simultaneously the particle composition in the flow as well as the bed.

To consider variation in particle size distributions in flow and bed, grain size is divided into  $k_e$  grades, and the diameter of the grade  $k$  grain is written  $d_k$ . Particles from grades  $k = 1$  to  $k = k_1$  are defined fine and considered to constitute a fluid phase if contained in the flow. Particles from grades  $k = k_1 + 1$  to  $k = k_e$  are defined coarse particles. The volumetric concentration of coarse and fine fractions, density of the interstitial muddy fluid, and mean diameter of the coarse particles in the flow respectively are expressed by

$$C_L = \sum_{k=k_1+1}^{k_e} C_k \quad (6)$$

$$C_F = \left( \sum_{k=1}^{k_1} C_k \right) / (1 - C_L) \quad (7)$$

$$\rho_m = \rho + \frac{\sigma - \rho}{1 - C_L} \sum_{k=1}^{k_1} C_k = \rho + (\sigma - \rho) C_F \quad (8)$$

$$d_{mL} = \left( \sum_{k=k_1+1}^{k_e} d_k C_k \right) / C_L \quad (9)$$

where  $\rho$  = water density,  $C_L$  = volumetric concentration of coarse particles in the flow,  $C_F$  = volumetric concentration of the fine particle fraction in the interstitial fluid,  $C_k$  = volumetric concentration of grade  $k$  particles in the total water and sediment volume.

The competence of the flow to transport sediment depends on the flow surface gradient. Herein, the majority of particles in the flow are considered too large to be suspended by the turbulence in the flow. Competence therefore is described by the following equilibrium concentration formulae (Takahashi, 1991):

If  $\tan \theta_w > 0.138$ , a stony type debris flow occurs, and

$$C_{L\infty} = \frac{\rho_m \tan \theta_w}{(\sigma - \rho_m)(\tan \phi - \tan \theta_w)} \quad (10)$$

If  $0.03 < \tan \theta_w \leq 0.138$ , an immature type debris flow occurs, and

$$C_{L\infty} = 6.7 \left\{ \frac{\rho_m \tan \theta_w}{(\sigma - \rho_m)(\tan \phi - \tan \theta_w)} \right\}^2 \quad (11)$$

If  $\tan \theta_w \leq 0.03$ , a turbulent water flow with bed load transport occurs, and

$$C_{L\infty} = \frac{(1 + 5 \tan \theta_w) \tan \theta_w}{\sigma / \rho_m - 1} \left( 1 - \alpha_0^2 \frac{\tau_{*c}}{\tau_*} \right) \left( 1 - \alpha_0^2 \sqrt{\frac{\tau_{*c}}{\tau_*}} \right) \quad (12)$$

where  $C_{L\infty}$  = equilibrium coarse particle concentration in the flow,  $\phi$  = internal friction angle of the sediment,  $\sigma$  = particle density, and

$$\tau_{*c} = 0.04 \times 10^{1.72 \tan \theta_w} \quad (13)$$

$$\alpha_0^2 = \frac{2 \{ 0.425 - (\sigma / \rho_m) \tan \theta_w / (\sigma / \rho_m - 1) \}}{1 - (\sigma / \rho_m) \tan \theta_w / (\sigma / \rho_m - 1)} \quad (14)$$

$$\tau_* = \frac{ht \tan \theta_w}{(\sigma / \rho_m - 1) d_{mL}} \quad (15)$$

in which  $\tau_{*c}$  = non-dimensional critical shear stress,  $\tau_*$  = non-dimensional shear stress,  $d_{mL}$  = mean diameter of movable coarse particles on the riverbed.

In the case of bed load transport, whether particles of diameter  $d_k$  are movable can be judged by a modification of Egiazaroff's critical shear stress concept:

$$\text{When } d_k / d_{mL} \geq 0.4, \quad \frac{u_{*ck}^2}{u_{*cML}^2} = \left\{ \frac{\log 19}{\log(19 d_k / d_{mL})} \right\}^2 \frac{d_k}{d_{mL}} \quad (16)$$

$$\text{When } d_k / d_{mL} < 0.4, \quad \frac{u_{*ck}^2}{u_{*cML}^2} = 0.85 \quad (17)$$

where  $d_{mL}$  = mean diameter of coarse particles on the bed surface,  $u_{*ck}$  = critical friction velocity of the  $k$  th grade particle,  $u_{*cML}$  = critical friction velocity of a particle whose diameter is  $d_{mL}$  ( $u_{*cML} = \sqrt{\tau_{*c}(\sigma / \rho_m - 1) g d_{mL}}$ ).

(3) Riverbed particle composition

Because the particle size composition of riverbed material is not necessarily the same as the particle size composition in a flow above the bed, composition in the flow will be changed by entrainment of bed material. To determine the particle size composition of runoff sediment, the particle composition of the riverbed with which the flow exchanges particles must be known.

Assuming that the total volume of grade  $k$  particles on a bed is  $V_k$ , the ratio of this grade's particles to the total particles (coarse plus fine ones) is

$$f_{bk} = \frac{V_k}{V_L + V_F} \quad (18)$$

where

$$V_L = \sum_{k=k_1+1}^{k_e} V_k, \quad V_F = \sum_{k=1}^{k_1} V_k \quad (19)$$

The ratio of grade  $k$  particles (grade  $k$  signifying coarse material) to the total coarse particles,  $f_{bLk}$ , is

$$f_{bLk} = \frac{f_{bk}(V_L + V_F)}{V_L} = \frac{f_{bk}}{\sum_{k=k_1+1}^{k_e} f_{bk}} = \frac{f_{bk}}{F} \quad (20)$$

If the ratio of the total coarse particles in the bed,  $F$ , satisfies

$$F \geq \frac{C_{*L}}{C_{*L} + C_{*F} - C_{*L} C_{*F}} \quad (21)$$

the coarse particles form a skeletal structure, and fine particles can be stored in its void spaces. In equation (21),  $C_{*L}$  is the volume concentration of all the coarse particles when the bed is composed only of coarse particles, and  $C_{*F}$  is that of fine particles when it is composed only of fine particles. For simplicity, both  $C_{*F}$  and  $C_{*L}$  are assumed to be 0.65, and the smallest  $F$  that satisfies equation (21) is 0.74. In this case, the volume ratio of the fine particles assumed to be stored only in the void space of the coarse particle framework,  $C_{*k}$ , is

$$C_{*k} = \frac{C_{*L}}{1 - C_{*L}} \frac{V_k}{V_L} = \frac{C_{*L}}{1 - C_{*L}} \frac{f_{bk}}{\sum_{k=k_1+1}^{k_e} f_{bk}}, \quad k = 1 \sim k_1 \quad (22)$$

When the ratio of the fine particles is greater than 26%, coarse particles can no longer form a skeleton and will lie scattered among the accumulated fine particles. These fine particles will form a skeletal structure with the volume concentration  $C_{*F}$ , but its void space will be too small to store coarse particles. In this case, the ratio of fine particles is

$$C_{*k} = \frac{f_{bk}C_{*F}}{1-F} \quad (23)$$

Then, the volume concentration of the coarse particle fraction on the bed is

$$C_{*L} = \frac{FC_{*F}}{C_{*F}F+1-F} \quad (24)$$

#### (4) Erosion and deposition velocity

The erosion velocity equation that can be used regardless the type of sediment transport; debris flow, immature debris flow, or bed load transport (Takahashi, 1991) is

$$\frac{i_{sbo}}{\sqrt{gh}} = K \sin^{3/2} \theta_w \left\{ 1 - \frac{\sigma - \rho_m}{\rho_m} C_L \left( \frac{\tan \phi}{\tan \theta_w} - 1 \right) \right\}^{1/2} \times \left( \frac{\tan \phi}{\tan \theta_w} - 1 \right) (C_{L\infty} - C_L) \frac{h}{d_{mL}} \quad (25)$$

where  $i_{sbo}$  = erosion velocity of a riverbed whose mean particle diameter is  $d_{mL}$ ,  $K$  = a constant, and  $g$  = acceleration due to gravity.

In debris flow and immature debris flow types, the largest particle that can be moved due to the effect of flow is assumed to have a diameter that is the same as the depth of flow. Under this assumption, if  $d_{k_{2+1}} > h > d_{k_2}$  is satisfied, the ratio of erodible coarse sediment is  $\sum_{k=k_1+1}^{k_2} f_{bLk}$ , and the bulk erosion velocity  $i_{sbo} \sum_{k=k_1+1}^{k_2} f_{bLk}$ . The substantial volume of coarse particles belonging to grades  $k_1 < k \leq k_2$  is  $C_{*L} f_{bLk}$ . The erosion velocity for each grade of particle when  $d_{k_{2+1}} > h \geq d_{k_2}$  is

$$\left. \begin{array}{l} k_1 < k \leq k_2; i_{sbk} = i_{sbo} f_{bLk} C_{*L} \sum_{k=k_1+1}^{k_2} f_{bLk} \\ k > k_2; i_{sbk} = 0 \end{array} \right\} \quad (26)$$

Under bed load transport type, the critical tractive force of flow determines the size of the erodible particles on the bed.

The erosion velocity of fine particles,  $k \leq k_1$ , is

$$i_{sbk} = i_{sbo} (1 - C_{*L}) C_{*K} \sum_{k=k_1+1}^{k_2} f_{bLk} \quad (27)$$

When the volumetric concentration of coarse particles,  $C_L$ , at a certain position is larger than the equilibrium concentration,  $C_{L\infty}$ , at that position, the coarse particles will be deposited on the riverbed. The excess volume of particles per unit area is  $h(C_L - C_{L\infty})$ . If this amount of sediment is deposited within the period  $(h/u)/\delta_d$ , deposition velocity is expressed by equation (28). The deposition velocity of each coarse particle grade is given by equation (29);

$$i_{sbo} = \delta_d \frac{C_{L\infty} - C_L}{C_{*L}} \frac{q}{h} \quad (28)$$

$$i_{sbk} = i_{sbo} \frac{C_k}{C_L} C_{*L_{max}} \cdot (k > k_1) \quad (29)$$

where  $\delta_d$  = a constant,  $C_{*L_{max}}$  = volume concentration of the coarse particles in the maximum compacted state, and  $u$  = mean flow velocity.

If settling due to its own density is neglected, the fine particle fraction mixed with water is considered to constitute a fluid phase and trapped within the voids of the coarse particle's skeleton formed by the deposition of coarse particles. Then, the deposition velocity for fine particles;  $k \leq k_1$ , is

$$i_{sbk} = i_{sbo} (1 - C_{*L_{max}}) \frac{C_k}{1 - C_L} \quad (30)$$

Erosion and deposition velocities in bulk that include void space are given by equations;

$$i_{sb} = \frac{1}{C_{*L}} \sum_{k=k_1+1}^{k_2} i_{sbk} \quad (31)$$

$$i_{sb} = \frac{1}{C_{*L_{max}}} \sum_{k=k_1+1}^{k_2} i_{sbk} \quad (32)$$

#### (5) Formulae describing flow discharge

The sediment concentration in a flow necessarily influences resistance to that flow. According to Takahashi (1991), the unit width discharge in stony debris flow is

$$q = \frac{2}{5d_{mL}} \left\{ \frac{g}{0.02} \frac{\sigma C_L + (1 - C_L)\rho_m}{\sigma} \right\}^{1/2} \left\{ \left( \frac{C_{*L}}{C_L} \right)^{1/3} - 1 \right\} h^{5/2} \tan^{1/2} \theta_w \quad (33)$$

For an immature debris flow it is

$$q = \frac{0.7\sqrt{g}}{d_{mL}} h^{5/2} \tan^{1/2} \theta_w \quad (34)$$

For turbulent water flow that transports bed load, it is given by Manning's formula;

$$q = \frac{1}{n_m} h^{5/3} \tan^{1/2} \theta_w \quad (35)$$

where  $q$  = the water plus sediment discharge per unit width. Equation (35) also is used for a flow laden with highly concentrated sediment that satisfies the condition  $h/d_{mL} \geq 30$ . This is because of the predominance of turbulence which suspends particles, in which case the resistance formula does not differ from that of water flow.

#### (6) Continuity equations

The continuity equation for the total volume of water plus sediment is

$$\frac{\partial h}{\partial t} + \frac{1}{B} \frac{\partial qB}{\partial x} = i_{sb} K_1 + \frac{q_s}{B} \quad (36)$$

where  $B$  = width of flow,  $i_{sb}$  = the erosion ( $i_{sb} > 0$ ) or deposition ( $i_{sb} < 0$ ) velocity,  $q_s$  = inflow discharge per unit length of channel, and  $K_1$  = a coefficient given as follows:

$$K_1 = C_{*L} + (1 - C_{*L}) \{ C_{*F} + (1 - C_{*F}) s_b \}; (i_{sb} > 0)$$

$$K_1 = 1; (i_{sb} \leq 0)$$

in which  $s_b$  = degree of saturation of the bed.

The continuity equation for each particle grade is

$$\frac{\partial C_k h}{\partial t} + \frac{1}{B} \frac{\partial q C_k B}{\partial x} = i_{sbk} + \frac{q_{sk}}{B} \quad (37)$$

where  $i_{sbk}$  = erosion or deposition velocity, and  $q_{sk}$  = flow rate of  $k$  th grade particles from the side banks per unit length of channel. Note that because  $i_{sbk}$  does not include void space, is not equal to  $i_{sb}$ .

Generally, in a river reach in which the canyon between steep side banks is wide, the flow width,  $B$ , is narrower than the canyon width,  $B_0$ . Even in such a reach, riverbed variation occurs laterally flat along the entire canyon bottom due to the stream channel shifting. Riverbed variation therefore is

$$\frac{\partial z}{\partial t} + \frac{B}{B_0} i_{sb} = 0 \quad (38)$$

where  $z$  = riverbed elevation.

#### (7) Variation of riverbed grain size

Exchange of particles on the bed with those in a flow is assumed to take place in the surface layer of a bed whose thickness is  $\delta_m$ . Variation in the ratio of grade  $k$  particles on the surface layer of the bed is

$$\text{For deposition: } \frac{\partial f_{bk}}{\partial t} = \frac{B}{B_0} \frac{i_{sb} J_0 f_{0k} - i_{sbk} - i_{sb} (J_0 - J) f_{bk}}{\delta_m J} \quad (39)$$

$$\text{For erosion: } \frac{\partial f_{bk}}{\partial t} = \frac{B}{B_0} \frac{-i_{sbk} + i_{sb} C_* f_{bk}}{\delta_m J} \quad (40)$$

where  $J$  = solids concentration in the bed's surface layer,  $J_0 = J$  in the lower layer beneath  $\delta_m$ . They are given by the equations

$$J = C_{*L} + (1 - C_{*L}) C_{*F} \quad (41)$$

$$J_0 = C_{*L0} + (1 - C_{*L0}) C_{*F0} \quad (42)$$

### 7.1.2 Application to the Camuri Grande River

Two comparable scale rivers, the Camuri Grande (23.8km<sup>2</sup>) and Miguelena (19.0km<sup>2</sup>) form the Camuri Grande River basin (Fig. 6). This basin was divided into 525 sub-basins for a flood runoff analysis, and the river channels divided into 1157 sections,

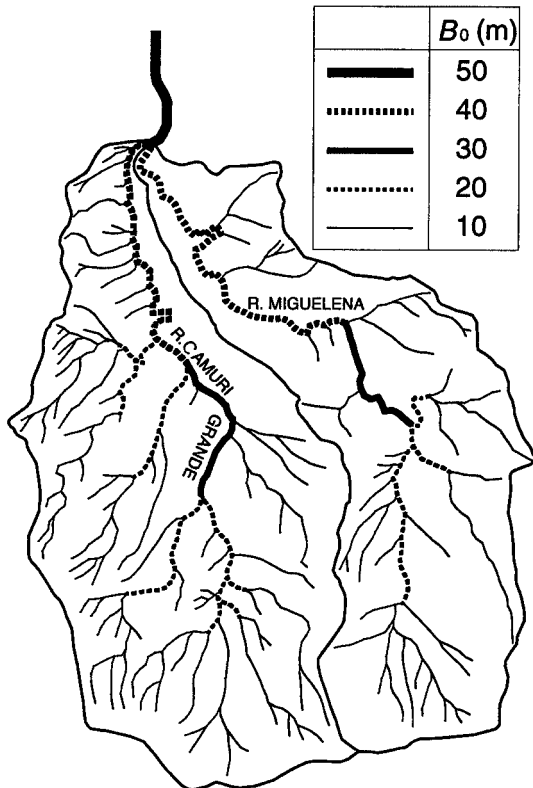


Fig. 6 River channel system and channel widths used in the simulation

$\Delta x = 100$  m, to calculate the various hydraulic quantities in each section. Canyon width,  $B_0$ , determined from aerial photographs and our reconnaissance data is distributed as in Fig. 6. Our field survey also found that before the flood the riverbed had stored sediment about 5m thick, whose particle size distribution is shown in Fig. 7. In the calculation, particle size was divided into 15 grades. The fraction smaller than 100  $\mu$ m (10% of the total particles) was considered the fine fraction which constitutes the muddy interstitial water.

The estimated rainfall intensities are given in Fig. 8 (Onda and Shibayama, 2001). Taking into account the amount of antecedent rainfall, the intensities in Fig. 8 are considered entirely effective to runoff.

The spatial grid-size in the calculation was set at  $\Delta x = 100$  m. Time intervals were changed depending on the flow velocity;  $\Delta t = 0.1$ s for velocities of 60cm/s or more,  $\Delta t = 0.2$ s for those of 40-60cm/s,  $\Delta t = 0.4$ s for 20-40 cm/s,  $\Delta t = 1$ s for 10-20cm/s,  $\Delta t = 2.5$ s for 5-10cm/s, and  $\Delta t = 5$ s for 0-5cm/s.

Values of the other quantities were set;  $C_* = C_{*L} = C_{*F} = C_{*Lmax} = C_{*Fmax} = 0.65$ ,  $\sigma = 2.65$  g/cm<sup>3</sup>,  $\rho = 1.0$  g/cm<sup>3</sup>,  $\tan \phi = 0.7$ , and  $\delta_m = 0.5$ m. The degree of saturation in the bed and Manning's roughness coefficient were set as  $s_b = 1.0$  and  $n_m = 0.03$  for  $B_0 > 50$  m;  $s_b = 0.8$  and  $n_m = 0.04$  for  $B_0 = 20-40$  m; and  $s_b = 0.8$  and  $n_m = 0.05$  for  $B_0 = 10$  m. The equivalent roughness coefficient on the slope,  $n_s$ , is assumed to be 1.0, and the coefficient in the formulas for the erosion and deposition velocities,  $K$  and  $\delta_d$ , respectively are assumed to be 0.5 and 0.0002. As the downstream boundary condition, the sea surface level 500m off the river mouth was set as constant.

Because the number of landslides was small, the sediment supply from the side banks was neglected, sediment runoff being attributed only to bed erosion.

Figure 9 shows temporal variations in the rates of flow and sediment runoff and in the mean diameters calculated at the con-

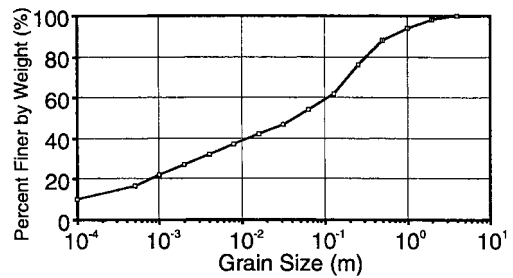


Fig. 7 Particle size distribution in the riverbed material

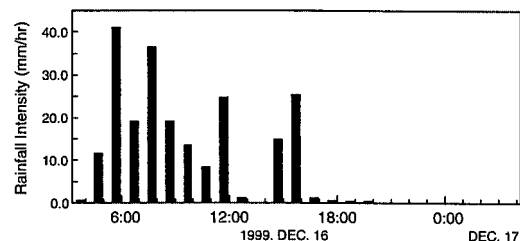


Fig. 8 Estimated hourly rainfall intensity in the Camuri Grande basin

fluence of the two rivers. A little before 6:00 a.m. on December 16, a debris flow ran out from the Camuri Grande River. It had a peak discharge of about 700m<sup>3</sup>/s and a sediment concentration almost equal to C<sub>s</sub>. A little after that there was a debris flow from the MiguELENA River which had a peak discharge of about 200m<sup>3</sup>/s. The durations of these debris flows were less than 30 minutes, and after them flash floods with comparatively thin sediment concentrations occurred for more than 10 hours. Mean particle size in the first debris flow was calculated as larger than 20cm. Although occasionally mean particle size in the after floods was large, generally it was 5 to 10cm, coinciding with the mean particle size of the riverbed.

Calculated longitudinal distributions of riverbed variations and the mean diameter on the surface of the riverbed along the main channel of the Camuri Grande River are given in Fig. 10. In this figure, t = 0 is 3:15 a.m. on 16 Dec. At t = 2h, severe erosion took place within the upstream river reach, but neither erosion nor deposition occurred in the downstream reach. The characteristic saw-tooth pattern reflects scattered junctions with tributaries at which locations runoff sediment is temporarily stored. At t = 4h, a rise in the riverbed of about 2m is seen from the river mouth to about 4km upstream. This agrees with our field investigation findings. The tendency for particle mean diameter to become small in the downstream reach also agrees with those findings. The calculated results, however, show that particles with a diameter larger than 1 meter are deposited at the river mouth, and such a large particle deposit actually occur at the fan-top. This discrepancy must be due to the neglect of particle segregation within the flow. That is, particle segregation within a debris flow concentrates the largest boulders at the forefront, which part is deposited at the fan-top.

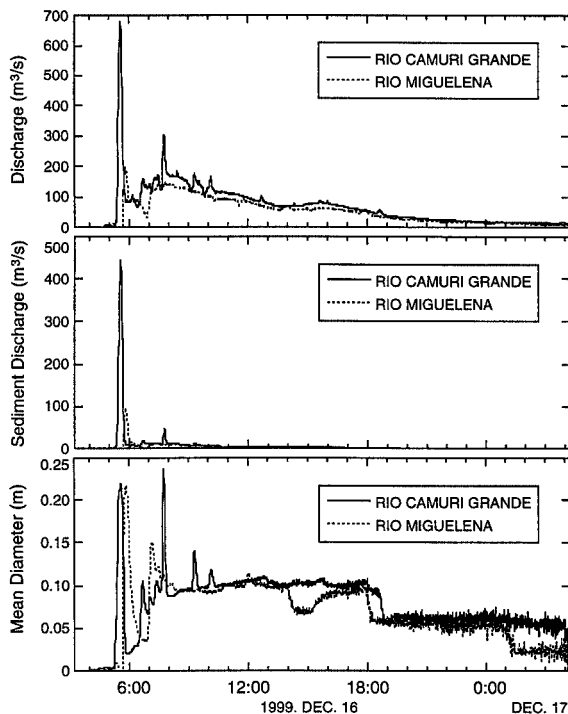


Fig. 9 Calculated results for hydrographs, sediment graphs and mean particle diameters of the two rivers

The calculated substantial volumes of sediment runoff from both rivers are shown in Fig. 11. The final substantial volume is 850 thousand cubic meters (bulk volume; 1,300 thousand cubic meters). The estimated volume deposited on the fan is 1,618,000m<sup>3</sup>, obtained by comparisons of the ground level of the fan before and after the flood. The difference is attributable to various causes; the error included in the estimation that uses ground levels, the premise of calculation that the thickness of the deposit on the riverbed before the flood is 5m, and the effects of landslides being neglected. Because the area of sediment deposition on the fan is about 0.79km<sup>2</sup>, the calculated runoff sediment volume is about 1.6m thick. This value has the feeling of reality as compared with impressions gained on the spot.

## 7.2 Reproduction of sediment flooding on the Camuri Grande fan

### 7.2.1 Fundamental equations

For the reproduction of sediment flooding, the fundamental equations are the depth-averaged two-dimensional momentum and continuity equations (Nakagawa and Takahashi, 1997):

$$\frac{\partial M}{\partial t} + \beta \frac{\partial(uM)}{\partial x} + \beta \frac{\partial(vM)}{\partial y} = \frac{\partial(z+h)}{\partial x} - \frac{\tau_{bx}}{\rho_T} \quad (43)$$

$$\frac{\partial N}{\partial t} + \beta \frac{\partial(uN)}{\partial x} + \beta \frac{\partial(vN)}{\partial y} = \frac{\partial(z+h)}{\partial y} - \frac{\tau_{by}}{\rho_T} \quad (44)$$

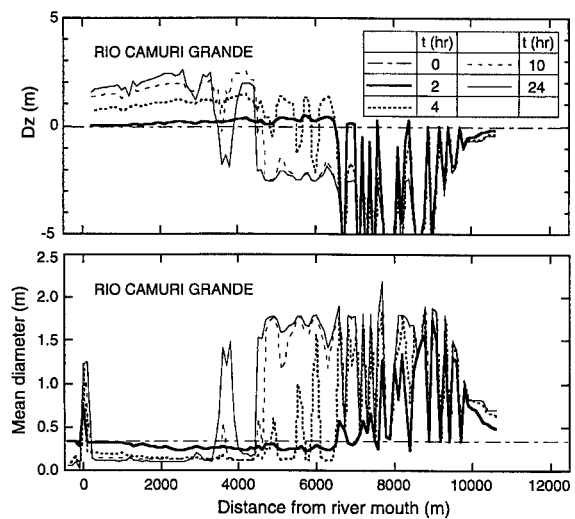


Fig. 10 Sequential time changes in longitudinal distributions of riverbed variation and in mean diameter

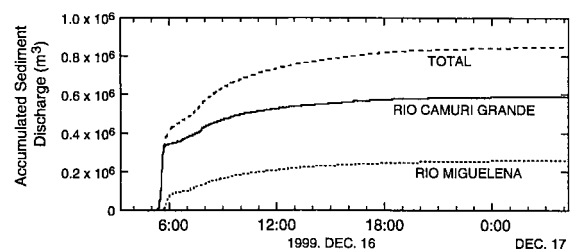


Fig. 11 Substantial sediment volume yields from the two rivers and their totals.

$$\frac{\partial h}{\partial t} + \beta \frac{\partial M}{\partial x} + \frac{\partial N}{\partial y} = i\{C_* + (1-C_*)s_b\} \quad (45)$$

The continuity of the coarse particle fraction sustained in the flow by the action of particle encounter is

$$\frac{\partial(C_h)}{\partial t} + \frac{\partial(CM)}{\partial x} + \frac{\partial(CN)}{\partial y} = \begin{cases} iC_{*L} & (i \geq 0) \\ iC_{*L_{\max}} & (i < 0) \end{cases} \quad (46)$$

The continuity of the fine particle fraction suspended in the interstitial fluid by turbulence is

$$\begin{aligned} \frac{\partial\{(1-C_L)C_F h\}}{\partial t} + \frac{\partial\{(1-C_L)C_F M\}}{\partial x} + \frac{\partial\{(1-C_L)C_F N\}}{\partial y} \\ = \begin{cases} i(1-C_{*L})C_{*F} & (i \geq 0) \\ i(1-C_{*L_{\max}})C_F & (i < 0) \end{cases} \end{aligned} \quad (47)$$

where  $M (= uh)$  and  $N (= vh)$  are the  $x$  and  $y$  components of the flow flux,  $u$  and  $v$  the  $x$  and  $y$  components of the mean velocity,  $\beta$  is the momentum correction coefficient,  $\tau_{bx}$  and  $\tau_{by}$  are the  $x$  and  $y$  components of the resistance to flow,  $\rho_T = \sigma C_L + (1 - C_L)\rho_m$ . With reference to equations (33), (34) and (35), the resistance terms are given by the following respective equations for stony debris, immature debris, and turbulent water flows:

$$\tau_{bx} = \frac{\rho_T}{8} \left(\frac{d_{mL}}{h}\right)^2 \frac{u\sqrt{u^2+v^2}}{\{C_L + (1-C_L)\rho_m/\sigma\} \{(C_{*L_{\max}}/C_L)^{1/3} - 1\}^2} \quad (48)$$

$$\tau_{bx} = \frac{\rho_T}{8} \left(\frac{d_{mL}}{h}\right)^2 \frac{v\sqrt{u^2+v^2}}{\{C_L + (1-C_L)\rho_m/\sigma\} \{(C_{*L_{\max}}/C_L)^{1/3} - 1\}^2} \quad (49)$$

$$\tau_{bx} = \frac{\rho_T}{0.49} \left(\frac{d_{mL}}{h}\right)^2 u\sqrt{u^2+v^2} \quad (50)$$

$$\tau_{by} = \frac{\rho_T}{0.49} \left(\frac{d_{mL}}{h}\right)^2 v\sqrt{u^2+v^2} \quad (51)$$

$$\tau_{bx} = \frac{\rho g n_m^2 u\sqrt{u^2+v^2}}{h^{1/3}} \quad (52)$$

$$\tau_{by} = \frac{\rho g n_m^2 v\sqrt{u^2+v^2}}{h^{1/3}} \quad (53)$$

Existing criteria for these flows are given by the gradient of the flow surface as discussed earlier.

A conservation equation of particle numbers is needed to account for variation in particle diameter in debris flows.

$$\frac{\partial}{\partial t} \left( \frac{C_L h}{\xi d_{mL}^3} \right) + \frac{\partial}{\partial x} \left( \frac{C_L M}{\xi d_{mL}^3} \right) + \frac{\partial}{\partial y} \left( \frac{C_L N}{\xi d_{mL}^3} \right) = \frac{i C_{*L_{\max}}}{\xi d_{mL}^3} \quad (54)$$

where  $\xi$  = shape factor of sediment particles and  $\xi d_{mL}^3$  = volume of a sediment particle.

Erosion and deposition velocities are given by equations (25) and (28), in which instead of  $\theta_w$ , the energy slope  $\theta$  is used;  $\tan\theta = \sqrt{\tau_{bx}^2 + \tau_{by}^2} / (\rho_T g h)$ .

The equation of change in the bed surface elevation is

$$\frac{\partial z}{\partial t} + i = 0 \quad (55)$$

## 7.2.2 Calculation method and the boundary conditions

The total area of the Camuri Grande fan was divided into arbitrary, unstructured mesh areas reflecting topographical conditions and the arrangement of buildings. For the calculation of the unknown variables in each mesh area (Fig. 12), variables  $M$ ,  $N$ ,  $u$ , and  $v$  were defined on the midpoints of the boundaries of the area, and variables  $h$ ,  $C_L$ , and  $z_b$  defined on the centroid of the area. The flow flux between the adjacent mesh areas of a particular area was calculated at the time step  $n, n+2, \dots$  and flow depths in the respective areas were calculated at the time step  $n+1, n+3, \dots$  using discretized fundamental equations; a leap-frog method. Herein, the finite volume expressions of fundamental equations are abbreviated (Takahashi et al., 2001b).

Figure 13 shows the adopted mesh division of 2,736 areas, as well as the thickness distribution of the deposit on the fan obtained by comparison of the two topographic maps (1/1,000), before and after the flood. The upper boundary of the figure is the coastline, the lower most two horn-like projections the inflow points of the Camuri Grande and Migelena rivers. The old river channel in the central part of the figure bends like a bow. A very thick deposit of more than 5m is on the left side of the old channel a little upstream of the river mouth. On the basis of our field observations, this is too thick and should be considered an error in the reading of the aerial photos. A thick cover of woods could cause such an error.

The hydrograph, sediment graph, and temporal variation in the mean particle diameter, obtained by the flood routing described earlier, are given as the input boundary conditions at the inflow points of each river.

A free-dropping type condition is used as the outflow boundary condition at the river mouth and at the shoreline;

$$M \text{ or } N = (2/3)^{3/2} h \sqrt{gh} \quad (56)$$

The constant time interval,  $\Delta t = 0.2s$  was used for the entire calculation period of 25 hours; 3:15 a.m., Dec. 16 to 4:15 a.m., Dec. 17. The numerical quantities in the calculation were  $\tan\phi = 0.7$ ,  $\sigma = 2.65 \text{ g/cm}^3$ ,  $C_{*DL} = 0.65$ ,  $\xi = 1.0$ ,  $\rho = 1.0 \text{ g/cm}^3$ ,  $n_m = 0.03$ , and  $\delta_d = 0.001$ .

## 7.2.3 Calculation results and discussion

Figure 14 shows the final calculation results for the deposit thickness distribution. In comparison to Fig. 13, the calculation

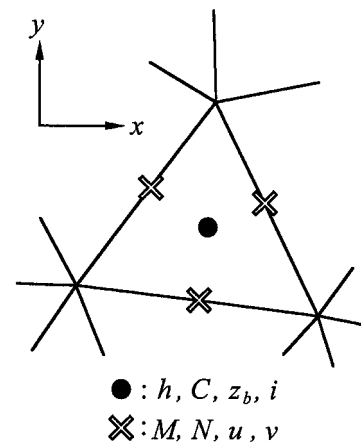


Fig. 12 Arrangement of variables on a mesh area

results tend to concentrate the flow in a narrower area along the old river channel and the overflow from that channel begins further upstream than it actually did. Flow and deposition along the mountain's foot adjacent to the western boundary of the fan and the flooding and deposition situations along the outer bank at channel bends, however, are well reproduced by the calculations. A conspicuous discrepancy is present in the northeast part of the fan. In the calculations, no sediment was deposited here, whereas in reality (Fig. 13) the deposit was thick. This discrepancy was not because of defective calculation, the actual deposition was due to sediment runoff from the basin that emerges from the mountain adjacent to this area.

### 7.3 Examination of the effectiveness of sabo dams and river improvement

There are various plans for coping with possible future debris flow hazards. The effectiveness of these plans can be assessed by

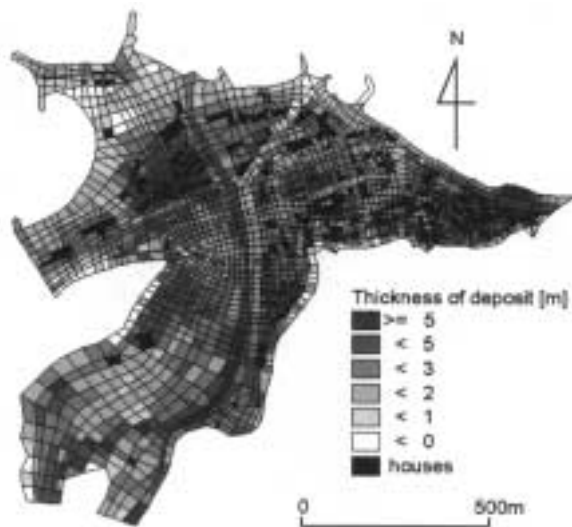


Fig. 13 Arrangement of mesh areas and distribution of the deposit thicknesses obtained from differences in elevation on maps before and after the flood

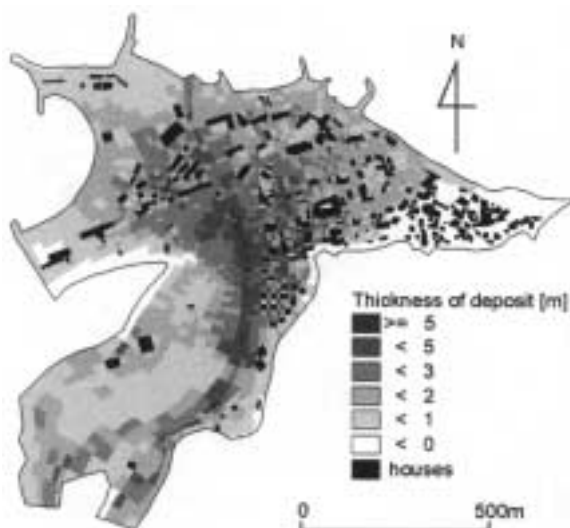


Fig. 14 Calculated results for the final stage

the numerical simulation method discussed earlier. One particular plan, the combination of sabo dams and channel works is considered. The conceptual arrangement is shown in Fig. 15.

#### 7.3.1 Effectiveness of sabo dams

(1) Method for taking into account in calculation the effect of a sabo dam

The method used to calculate the hydrograph, sediment graph, and particle composition at the fan-top is one-dimensional routing, described in 7.1. The sabo dam is set at the calculation point of flow discharge per unit width,  $q(i)$  (Fig. 16). Elevation of the dam crown,  $z1$ , is set equal to the sum of the mean bed elevation,  $\{z(i-1) + z(i)\} / 2$ , and the dam's height. The flow surface gradient,  $\theta_e$ , and effective flow depth,  $h'$ , are substituted into equations (33), (34) or (35) to calculate  $q(i)$ ;

$$\theta_e = \tan^{-1} \left\{ \frac{[z(i)+h(i)-z1]}{(\Delta x/2)} \right\} \quad (57)$$

$$h' = \begin{cases} h(i)+z(i)-z1 & ; h(i)+z(i)-z1 > 0 \\ 0 & ; h(i)+z(i)-z1 \leq 0 \\ h(i) & ; z(i) > z1 \end{cases} \quad (58)$$

The notations in these equations appear in Fig. 16.

The gradient,  $\theta_e'$ , needed to calculate the equilibrium sediment

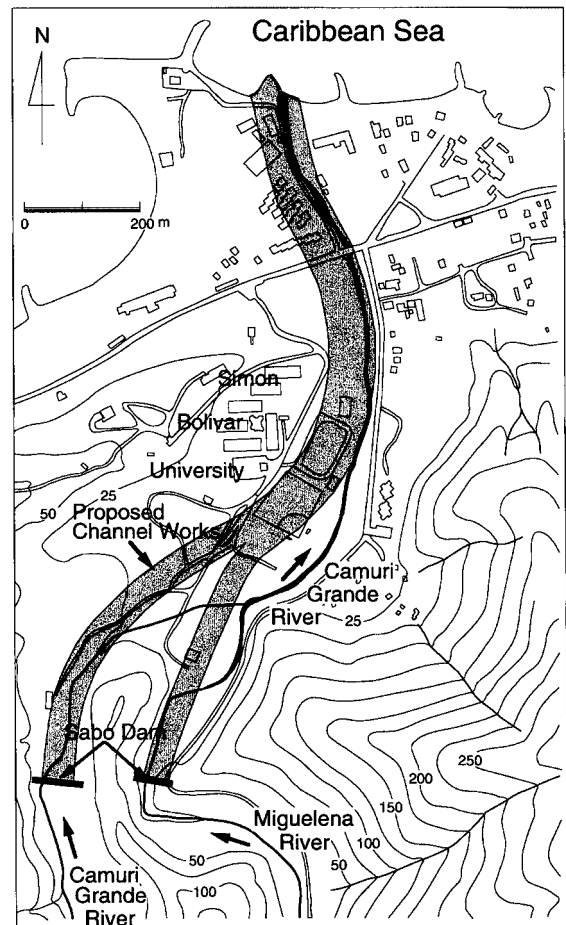


Fig. 15 Location of sabo dams and plan view of the channel works

concentration,  $C_{L\infty}$ , is evaluated by

$$\theta_e' = \tan^{-1} \left\{ \frac{[z(i) - z1]}{(\Delta x/2)} \right\} \quad (59)$$

When  $\theta_e'$  is less than zero, the equilibrium concentration is set at zero.

(2) Calculation conditions and results

Three cases were examined. In case 1, no dam is set in the Camuri Grande or Miguelena rivers. In case 2, both rivers have 10m high sabo dams, one per river. In case 3, the Camuri Grande has a 20m high sabo dam, and the Miguelena a 10m high one.

In cases 1 and 2, canyon width is assumed to be 100m in the reaches 300m immediately upstream of each dam, whereas in case

3 the 400m reach just upstream of the 20m high sabo dam in the Camuri Grande River is assumed to be 100m wide. The flow width in these reaches is assumed to be equal to the canyon width.

The same rainfall as in the reproduction of phenomena described in 7.1 is given.

The calculated flow hydrograph, sediment graph, and mean diameter of the runoff sediment at the dam sites are shown in Fig. 17 for case 3. A comparison of Fig. 17 with Fig. 9, which gives the results for case 1, shows that a sabo dam can cut off the sharp, large peak of the debris flow front. The peak flow rate in the Camuri Grande River without the sabo dam (case 1) is about 700m<sup>3</sup>/s, whereas with construction of a 20m high sabo dam it is decreased to about 300m<sup>3</sup>/s, and the debris flow front that comes out at about 6:00 a.m. is completely trapped by the dam. For case 2, although the peak discharge is decreased to about 550 m<sup>3</sup>/s the debris flow front can not be completely cut off.

The peak sediment discharge of the debris flow front with no dam in the Camuri Grande River is about 450 m<sup>3</sup>/s. Because the debris flow front is completely cut off in case 3, the peak sediment discharge is markedly decreased, to about 40 m<sup>3</sup>/s.

Table 1 shows the effects of sabo dams in terms of sediment volume yields on the fan area.

7.3.2 Effectiveness of the combination of sabo dams and channel works

Although sabo dams are very effective for reducing the peak discharge as well as peak sediment discharge, sediment vol-

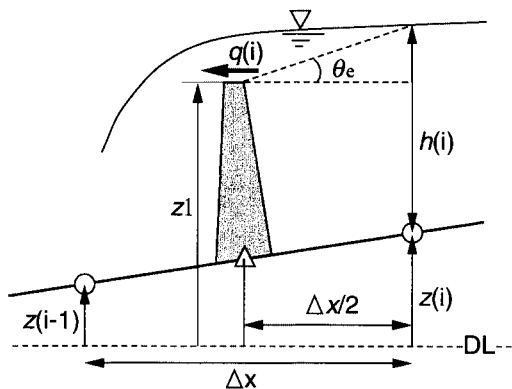


Fig. 16 Definition of the gradient used in calculating the discharge over the dam

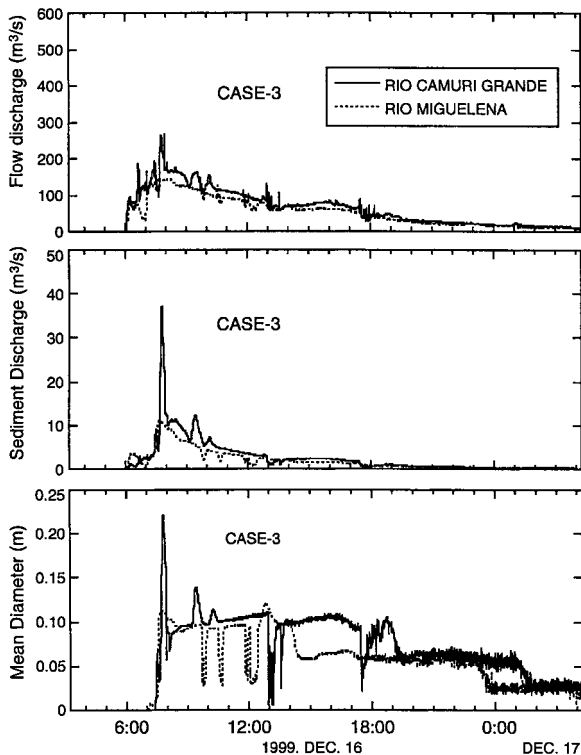


Fig. 17 Calculated hydrograph, sediment graph and mean diameter of the overflows of sabo dams on the two rivers

CASE	CASE-1		CASE-2		CASE-3	
	Vout* (m³)	Vout (m³)	Vout-cut** (%)	Vout (m³)	Vout-cut (%)	
Camuri Grande	912,000	686,000	24.8	317,000	65.2	
Miguelena	397,000	223,000	43.8	223,000	43.8	
Total	1,309,000	909,000	30.6	540,000	58.7	

\*Vout : sediment volume outflow from the Sabo dam  
 \*\* Vout-cut = (Vout (case-1) - Vout) / Vout (case-1) x 100

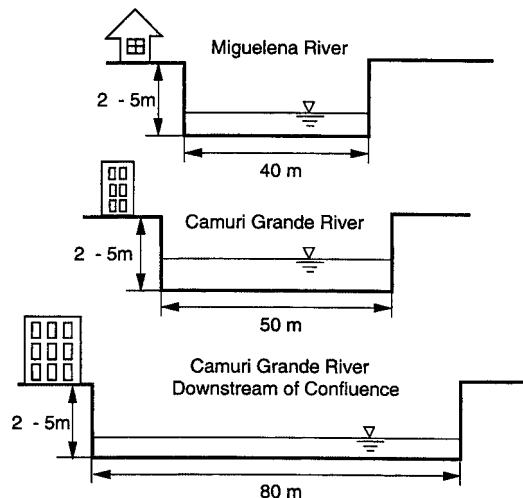


Fig. 18 Channel cross-sections

umes flowing out of the dams are still large. Unless larger dams are built, countermeasures such as channel works must be introduced to prevent sediment flooding.

The combination of sabo dams and channel works therefore was considered. The plan view of the channel works is shown in Fig. 15. Cross-sections of the channels in the Miguelena and Camuri Grande rivers and of the Camuri Grande River downstream of the confluence are shown in Fig. 18. Longitudinal profiles of the channel bed elevations are given in Fig. 19. The unstructured mesh for the calculation of flooding and deposition on the fan, as well as inside the channel, was altered from that in the previous section to fit the new channel alignment.

Five different combinations were examined (Table 2). In case 1 there is no sabo dam but channel works 2m deep exist. Case 4 has the combination of 20m high and 10m high sabo dams in the respective rivers, and channel works 3m deep. Referring to cases 1 and 4, the conditions for other cases are clear in Table 2.

The inflow boundary conditions are those for cases 1 to 3 in the previous section that correspond to the respective dam conditions.

An imaginary sea basin is provided as the outflow boundary condition near the river mouth. Sedimentation due to the settling of particles is considered when the settling velocity of each particle diameter becomes larger than the local shear velocity in the basin.

Figure 20 shows the deposition area pattern and the deposit thickness distributions in the cases at the final stage ( $t = 25$  h). The sediment deposit area and thickness of the deposit are much greater in case 1, in which no sabo dam exists and the depth of channel is shallow (2m). Because the channel can not store the total sediment volume of 1,309,000 m<sup>3</sup>, the materials of both rivers, water and sediment, overflow the channel, and there are some places in the channel where the thickness of the deposit is

more than 5m. This suggests that, if the scale of a flood is comparable to that in 1999, even were very wide channel works constructed, flooding and deposition of sediment would be inevitable without an appropriate scale of sabo dams.

In case 2, the calculated sediment deposit area is very similar to that in case 1, but the thickness of the deposit in the channel is less. In case 3, the sediment deposit area is decreased and the thickness of deposit as well. As a deposit area remains on the fan, the channel works need to be deepened. As a method to deepen the channel, dredging would not be effective because of the limitation of downstream elevation imposed by the sea. The ground elevations of the mesh areas adjacent to the channel, raised as embankment, therefore were evaluated.

For a minimum channel depth of 3m (case 4), the sediment deposit area and thickness of the deposit are very similar to case 3. A wide deposit area exists downstream of the channel, because sedimentation near the river mouth is affected by the sea level.

In case 5, little flooding or sediment deposition occur on the fan area. At the few places flooding does occur, local protection by raising the embankment would be most suitable.

### 8. CONCLUSIONS

The 1999 Venezuelan sediment disaster was caused neither by the unprecedented severity of the rainfall nor the unexampled volume of sediment runoff in history. Comparable natural phenomena have been recorded in Japan; for example, the Great Hanshin Flood of 1938. The resulting Venezuelan disaster, however, is one of the most disastrous events on record in view of the number of casualties.

The natural and social factors that resulted in such numerous casualties were analyzed. Poor natural conditions, deeply weathered geological formations and very steep topography, are combined with the chance to earn money in the central part of the state of Vargas. Because of these conditions, numerous low-income people live illegally in very hazardous areas in which even slightly adverse conditions can cause disasters.

Japanese experiences suggest that intensive sabo works can remarkably reduce the chance of disaster. We consider that similar sabo works, a combination of sabo dams and channel works, would be effective for mitigating disasters on the Camuri Grande fan area.

We propose a numerical simulation method that reproduces the hazards on that fan area that uses only the rainfall, topography, and existing sediment conditions in the river reaches as a tool to assess the effectiveness of these sabo plans. This method was validated by a comparison of the calculated results and actual observations.

Possible sabo plans were assessed by this simulation method, and an appropriate plan was proposed.

### ACKNOWLEDGMENTS

This work was supported by a Grant-in-Aid of Scientific Research, No.11800020, from the Japanese Ministry of Education, Science, Sports and Culture. The field work was done by T. Takahashi, H. Nakagawa, M. Chigira, Y. Onda, N. Maki, J. Aguirre-Pe and E. Jauregui.

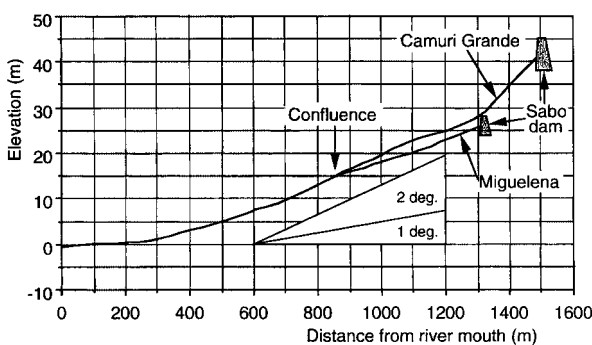


Fig. 19 Longitudinal channel work profiles

Table 2. Calculation conditions

CASE NO.		CASE-1	CASE-2	CASE-3	CASE-4	CASE-5
SABO WORKS						
SABO DAM (HEIGHT)	CAMURI	NO	10 m	20 m	20 m	20 m
	MIGUELENA	NO	10 m	10 m	10 m	10 m
CHANNEL WORKS	BANK HEIGHT	2m	2m	2m	3m	5m

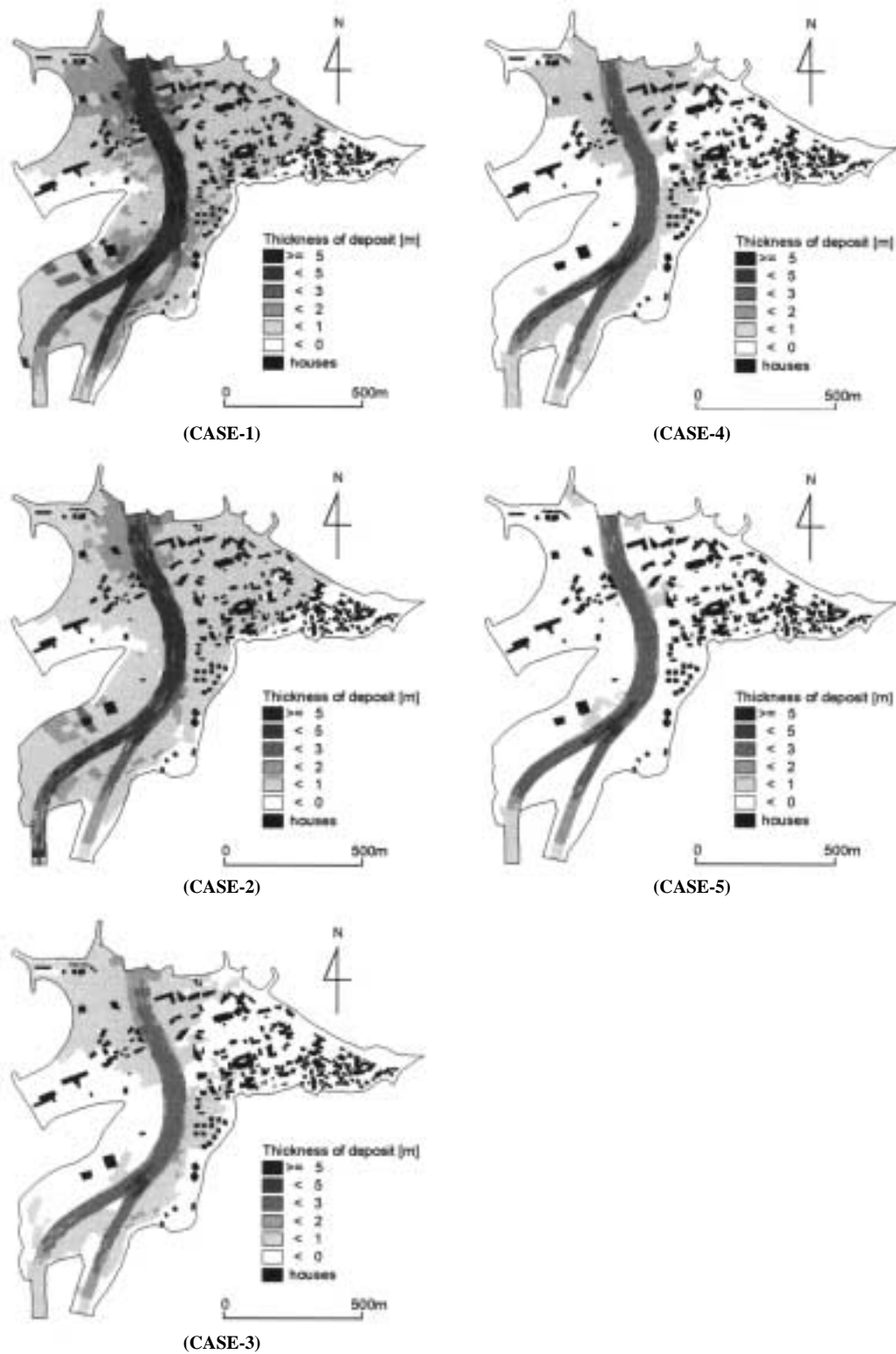


Fig. 20 Calculated results for particular cases

Special thanks are owed to I. Okano, a JICA expert attached to the Venezuelan Ministry of Environment and Natural Resources, for the arrangement of the necessities for doing the field work and for the preparation of various data. Sincere thanks are given to A. Carrillo of the Ministry of Environment and Natural Resources, Venezuela for his active cooperation and leadership in the field work.

R. Leonett, Vice-Minister and B. Norys, Advisor of the Ministry of Environment and Natural Resources, Venezuela made our investigation possible, and the Japanese Embassy in Caracas provided the conveniences for the field survey.

### NOMENCLATURE

$B$  : stream channel width  
 $B_0$  : canyon width  
 $C_k$  : volumetric concentration of grade  $k$  particles in the total volume of water and sediment  
 $C_F$  : volumetric concentration of the fine particle fraction in the interstitial fluid  
 $C_L$  : volumetric concentration of coarse particles in the flow  
 $C_{L\infty}$  : equilibrium coarse particle concentration in the flow  
 $C_s$  : volumetric particle concentration in the static bed  
 $C_{sF}$  : volumetric concentration of all the fine particles when the bed is composed only of the fine particles  
 $C_{sF0}$  :  $C_{sF}$  in the lower bed layer  
 $C_{sk}$  : volumetric concentration of grade  $k$  particles in the bed  
 $C_{sL}$  : volumetric concentration of all the coarse particles when the bed is composed only of coarse particles  
 $C_{sL\max}$  : volumetric concentration of the coarse particles in the maximum compacted state  
 $C_{sL0}$  :  $C_{sL}$  in the lower bed layer  
 $d_k$  : diameter of grade  $k$  particle  
 $d_{mL}$  : mean diameter of coarse particles in the flow  
 $d_{mL}^{\dagger}$  : mean diameter of movable coarse particles on the riverbed  
 $f_{bk}$  : volume ratio of grade  $k$  particles to all particles existing on the bed  
 $f_{bLk}$  : volume ratio of grade  $k$  particles to all coarse particles existing on the bed  
 $F$  : volume ratio of the coarse particle fraction to all particles on the bed  
 $g$  : acceleration due to gravity  
 $h$  : flow depth  
 $h'$  : effective flow depth  
 $i_{sb}$  : bed erosion or deposition velocities in bulk  
 $i_{sbk}$  : erosion or deposition velocities of grade  $k$  particles on the bed  
 $i_{sbo}$  : erosion or deposition velocities on a riverbed comprised of particles with the mean diameter  $d_{mL}$   
 $J$  : solids concentration on the surface layer of the bed  
 $J_0$  :  $J$  in the lower bed layer beneath  $\delta_m$   
 $k$  : grade of particle diameter  
 $k_1$  : largest diameter grade of fine particles  
 $k_c$  : largest diameter grade of coarse particles  
 $K$  : a numerical coefficient

$M$  :  $x$  component of the flow flux  
 $n_e$  : equivalent roughness coefficient of the slope  
 $n_m$  : Manning's roughness coefficient of the riverbed  
 $N$  :  $y$  component of the flow flux  
 $q$  : water or debris flow discharge per unit width of the river channel  
 $q_s$  : water flow discharge per unit width on the slope  
 $q_{sk}$  : inflow rate of grade  $k$  particles from side banks per unit length of channel  
 $r_e$  : intensity of effective rainfall  
 $s_b$  : degree of bed saturation  
 $t$  : time  
 $u$  : flow velocity  
 $u_{*ck}$  : critical friction velocity of grade  $k$  particles  
 $u_{*cML}$  : critical friction velocity of a particle whose diameter is  $d_{mL}$   
 $v$  :  $y$  component of the flow velocity  
 $V_F$  : total volume of fine particles on the bed  
 $V_k$  : total volume of grade  $k$  particles on the bed  
 $V_L$  : total volume of large particles on the bed  
 $x$  : longitudinal distance  
 $y$  : lateral distance  
 $z$  : riverbed elevation  
 $z1$  : elevation of dam crown  
 $\alpha_k$  : a coefficient defined by eq.(2)  
 $\alpha_o$  : a coefficient defined by eq.(14)  
 $\beta$  : momentum correction factor  
 $\delta_d$  : a numerical constant  
 $\delta_m$  : thickness of the particle exchange layer  
 $\xi$  : shape factor of sediment particle  
 $\theta$  : energy slope  
 $\theta_s$  : slope gradient  
 $\theta_w$  : water surface gradient  
 $\rho$  : density of water  
 $\rho_m$  : apparent density of the interstitial fluid  
 $\rho_T$  : apparent density of the flowing material  
 $\sigma$  : density of particles  
 $\tau_{bx}$  :  $x$  component of resistance to flow  
 $\tau_{by}$  :  $y$  component of resistance to flow  
 $\tau_s$  : non-dimensional shear stress  
 $\tau_{sc}$  : non-dimensional critical shear stress  
 $\phi$  : internal friction angle

### REFERENCES

- Chigira, M., 2001. 1999 landslide disasters in Venezuela. In: Flood and Sediment Disasters Caused by the 1999 Heavy Rainfall in Venezuela, Research Report on Natural Disasters, DPRI, Kyoto University, Kyoto, 7-14.
- Maki, N., 2001. Damage and disaster response on the 1999 flood and sediment disasters in Venezuela. In: Flood and Sediment Disasters Caused by the 1999 Heavy Rainfall in Venezuela, Research Report on Natural Disasters, DPRI, Kyoto University, Kyoto, 77-96.
- Mizuyama, T., 1985. Concept of debris flow. In: Prediction and Countermeasures for Sediment Disasters, Japanese Society of Soil Mechanics and Foundation Engineering, Tokyo, 249-256 (in Japanese).
- Nakagawa, H. and Takahashi, T., 1997. Estimation of a debris flow hydrograph and hazard area. Proc. 1st International Conference on Debris

- Flow Hazard Mitigation, ASCE, 64-73.
- Onda, Y. and Shibayama, T., 2001. Rainfall and Landslide Distribution on Naiguata River and Camuri Grande on the 1999 Disaster in Venezuela. In: Flood and Sediment Disasters Caused by the 1999 Heavy Rainfall in Venezuela, Research Report on Natural Disasters, DPRI, Kyoto University, Kyoto, 1-6.
- Takahashi, T., 1991. Debris Flow. Balkema, Rotterdam, 1-165.
- Takahashi, T., Chigira, M., Nakagawa, H., Onda, Y., Maki, N., Aguirre-Pe, J. and Jauregui, E., 2001. Flood and Sediment Disasters Caused by the 1999 Heavy Rainfall in Venezuela, Research Report on Natural Disasters, DPRI, Kyoto University, Kyoto, 1-141.
- Takahashi, T., Nakagawa, H. and Satofuka, Y., 2001a. Estimation of debris-flow hydrograph in the Camuri Grande River basin. In: Flood and Sediment Disasters Caused by the 1999 Heavy Rainfall in Venezuela, Research Report on Natural Disasters, DPRI, Kyoto University, Kyoto, 41-50.
- Takahashi, T., Nakagawa, H., Satofuka, Y. and Kawaike, K., 2001b. Reproduction of the flooding and deposition of debris flow on the fan of Camuri Grande. In: Flood and Sediment Disasters Caused by the 1999 Heavy Rainfall in Venezuela, Research Report on Natural Disasters, DPRI, Kyoto University, Kyoto, 51-61.
- USGS-CINDI (Center for Integration of Natural Disaster Information) team, 1999. Venezuelan disaster December. <http://cindi.usgs.gov/venezuela/venezuela>.